Carbon 183 (2021) 84–92

Contents lists available at ScienceDirect

Carbon

journal homepage: www.elsevier.com/locate/carbon

Research Article

Formation of graphene nanostructures using laser induced vaporization of entrapped water

Sukhyun Hong, Minsuk Park, Soonhyung Kwon, Jehyun Oh, Sungmin Bong, Balu Krishnakumar, Sang-Yong Ju*

Department of Chemistry, Yonsei University, 50 Yonsei-ro, Seodaemun-Gu, Seoul, 03722, South Korea

ARTICLE INFO

Article history:
Received 9 April 2021
Received in revised form
1 June 2021
Accepted 26 June 2021
Available online 8 July 2021

Keywords:
Graphene
Entrapped water
Vaporization
Nanoballoon
Laser irradiation

ABSTRACT

Facile construction of graphene nanostructures are potentially important for fundamental studies and various applications owing to its transparency and mechanical strength. Here we found that focused laser irradiation of a graphene/entrapped water/hydrophobic substrate leads to vaporization of entrapped water and consequent formation of graphene nanostructures. Graphene mechanically exfoliated on a hydrophobicized Si substrate was served as a transformable and impermeable nanocontainer in which water anisotropically and slowly diffuses from the weak edges into the van der Waals (vdW)-coupled interstitial volume between graphene and the substrate. Time-lapsed Raman mappings show that water entrapment promotes progressive lowering of the frequencies of the G and 2D bands of graphene and exhibits slower diffusion owing to vdW decoupling of substrate-induced doping and biaxial strain of graphene with hydrophobic substrate. Moreover, vaporized entrapped water promotes nanostructures by graphene sliding and bulging actions. This methodology represents viable approach to produce nanostructures from two dimensional materials.

1. Introduction

Nanochannel have dimensions that approach the hydrodynamic radii of fluids as compared to microchannels, yet both require multiple photolithographic steps for the preparations. Thus, it is possible to maximize fluid-solid interfaces and efficiently control flow of charged liquid by modifying surface chemical functionality [1–3]. For these reasons, nanochannels have been utilized in protocols for sorting charged biomaterials such as proteins [4,5] and DNA [6], and in microfluidic systems for delivering and reacting small volumes of various fluids.

Graphene, consisting of an atom thick honeycomb lattice of sp^2 carbons, exhibits excellent mechanical strength [7], optical transparency [8] and flexibility [9], and large area producibility by chemical vapor deposition method [10]. Like carbon nanotube [11–13], graphene has a minimum surface frictional force with water and gases owing to a lack of surface chemical functionality. This property enables a fast flow of fluids, especially water [14,15]. Moreover, specific modification of its surface enables graphene to be utilized to selectively locate an ion in confined geometry [16–18]. These properties make graphene as an ideal platform for nanofluidic systems. As a result, new approaches that enable the fabrication graphene nanostructures are required to facilitate fundamental studies of water, and for various applications including biosensing [19], material transport [20,21], drug delivery [22,23], and diagnostic devices [23].

The formation of graphene nanochannels has been reported by several groups [24–31]. One study showed random nanochannels are formed by diffusion of water between graphene and a hydrophilic SiO_2 substrate followed by drying [26]. Xie and coworkers [24] demonstrated that graphene nanochannels can be formed by a transferring graphene film to a prepatterned silicon wafer template and that the channels are responsible for the enhancement in ionic conductance over that of the silicone substrate. Moreover, Mirsaidov and coworkers [25] reported that graphene channels with widths of few tens of nanometer can be generated by surface energy-driven spontaneous scrolling of hydrophobic graphene upon contact with water. Most recently, its was shown simple drying can be utilized to form random graphene wrinkles that contains water with a phase behavior being different from that of bulk water [27]. Unfortunately, the former suffers from a time-consuming multistep photolithographic procedure along with

* Corresponding author.
E-mail address: syju@yonsei.ac.kr (S.-Y. Ju).

https://doi.org/10.1016/j.carbon.2021.06.071
0008-6223/

giving only micrometer channel widths, and the latter approach lacks control over the positions and sizes of the formed nanochannnels. Consequently, the development of a simple method to form graphene nanochannel in a controlled manner is a highly desirable endeavor.

On the other hands, the investigation of entrapped water at the two dimensional interface between graphene and hydrophilic surface such as mica and SiO_2/Si substrate have been extensively studied in details [32–36]. Those studies suggest that confined water exhibits ice-like water structure within confined nanometer space and isotropically diffuses. However, interfacial behavior of water in graphene on hydrophobic substrate was not studied systematically.

In the investigation described below, we found that graphene nanostructures can be formed in a controlled manner by using focused laser irradiation of water entrapped between the graphene/substrate sandwich structure. The procedure for graphene nanostructure generation involves three stages beginning with water diffusion into interstitial areas between graphene and a hydrophobic substrate, followed by laser beam promoted vaporization of the entrapped water, and final upward bulging and sliding of the graphene to form 5–20 nm high and a few hundred nanometer wide nanochannels and nanoballoons. In the course of this process, liquid-like diffused water decouples strong interaction between graphene and the hydrophobic substrate, which leads to partial floating of the graphene and consequent sliding to produce nanostructure.

2. Experimental

2.1. Materials and instrumentations

All reagents are of spectroscopic grade and used without further purification. Mechanical exfoliation of highly crystalline kish graphite flake (Toshiba, Japan) was performed by using Scotch tape. Silicon with 285 nm thick SiO_2 (Lot #:7400383-603-Z, Shinetsu, Japan) were utilized as a substrate for mechanically exfoliating graphene. Scotch tape with exfoliated graphene was attached on the center of substrate, and vacuum annealing at 120 °C for 10 min was performed to improve graphene adhesion, inducing ω_G and ω_{2D} upshifts, and to release trapped gas at graphene-substrate interface [37]. Millipore quality DI water with a resistivity greater than 18 MΩ was used in all experiments. Bare and octadecyltrichlorosilane (OTS)-functionalized substrate (ODS), used as respective hydrophilic and hydrophobic silicon substrates, were prepared by using the following methods. Bare SiO_2 substrate was prepared by sequential washing with methanol, acetone and isopropanol, followed by application of a N_2 stream. ODS was made by using self-assembled monolayer formation on O_2 plasma cleaned SiO_2/Si substrate (100 W power, O_2 = 20 sccm, 0.30 Torr, 60 s), a step necessary for enabling full coverage of OTS on SiO_2 [38]. Plasma cleaned SiO_2 substrate was immersed in 10 mM OTS solution in dry toluene, which was obtained by treating with 4 Å molecular sieve. The substrate was washed with toluene and dried with a N_2 stream to produce ODS. It is noteworthy that both ODS in water and graphene/ODS without water does not have any noticeable damage after focused laser irradiation whose intensity varies from 0.5 mW to 65 mW up to 30 s (Figs. S1a and b for ODS in water and Figs. S1c and d for graphene/ODS), judged by AFM topography. However, prolonged 50 mW exposure for 3 min on graphene/ODS without water resulted in graphene hole (Figs. S1e and f). Microscopes and objective lenses were purchased from Olympus (Japan). Other optical elements such as convex lenses and bandpass filters were purchased from Thorlabs (NJ, USA). Optical microscope measurements were conducted using an upright microscope (BX51) equipped with 100× objective lens (numerical aperture (NA) = 0.90) and a CMOS camera (3.6 μm/pixel, 1280 × 1024, DCC1645C, Thorlabs, NJ, USA). AFM topographies were obtained by using JPK nanowizard (Switzerland) *via* tapping mode. A silicon cantilever (force constant: 37 N/m, ACTA-20, App Nano, CA, USA) was utilized with a resonance frequency of 300 kHz. Quoted radius of curvature from AFM tip is 6 nm. Especially, presence of residual adhesive and layer information during graphene exfoliation was obtained by collecting a reflection image of the sample using a charge-coupled device (CCD) (4.54 μm/pixel, 1940×1460, CoolSNAP MYO, Teledyne Photometrics, AZ, USA) with 100× objective (NA = 0.90) and 550 nm bandpass filter (FWHM = 10 nm, FB550-10) in the emission side of upright microscope. Typically, differential reflectance values of SLG, obtained by subtracting sample reflectance from substrate reflectance divided by substrate reflectance, are below 0.08 and are free from contributions from residual adhesive, which in good agreement with our previous report [39]. SEM images were acquired by using field emission SEMs (SU8000, Hitachi or 7610f-plus, JEOL Ltd., Japan) operating at 5 kV as an acceleration voltage.

2.2. Water diffusion experiments

Monitoring of water diffusion was performed in an O-ring sealed cell chamber (SC15032, Aireka Cells, Aireka Scientific Co., Ltd, Hong Kong) which allows measurements to be made on graphene through a pair of piranha-cleaned round-shaped coverslips (thickness: 0.20 mm, Lot. 30474819, Marienfeld, England) at 25 °C (Fig. 1c and d). Special care was taken to maintain ultraclean chamber, whose surface and contacts with the graphene surface were thoroughly cleaned using cotton balls. Exfoliated graphene on ODS was elevated to near the focal length of objective on an anodized block placed in cell chamber filled with water. The top lid was carefully placed on the cell chamber to avoid any trapped bubble formation. Using this setup, long term Raman mappings were performed over periods of few tens of days.

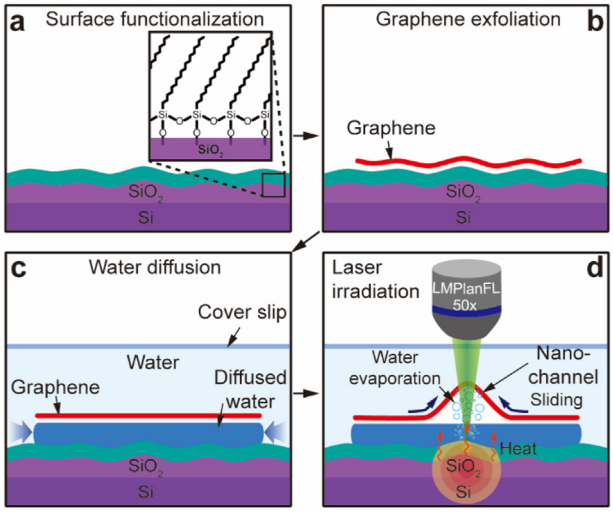

Fig. 1. Graphene nanostructure formation by using laser irradiation promoted vaporization of water entrapped between graphene and ODS. (a) OTS functionalization of O_2 plasma-treated 285 nm thick SiO_2/Si substrate. Note that SiO_2/Si has innate roughness. (b) Graphene exfoliation on ODS. (c) Water diffusion into interspace between graphene and ODS in a viewport-containing water chamber. (d) Laser-assisted heating and vaporization of the entrapped water, and subsequent formation of graphene nanostructures by bulging and sliding.

2.3. Raman measurement and nanostructure formation

Layer number, stain, and doping of exfoliated graphene were examined by using Raman spectroscopy. A custom-made Raman spectrometer on an optical microscope with a 532 nm laser using backscattering geometry was utilized to obtain graphene scattering signals as described previously [39]. The scattered light was collected with a 100× objective (NA = 0.9), and dispersed by Triax 320 (focal length = 320 mm, Horiba, Japan) with a grating of 1800 g/mm, leading to approximately 0.8 cm^{-1} resolution. The laser spot size based on beam waist is *ca.* 1 μm. For nanochannel formation, laser power of 0.5 mW was utilized. The spectrometer was calibrated with several lines (365.015, 404.656, 435.833, 546.074, and 579.066 nm) of an Hg/Ar lamp peak with polynomial fitting by using a Hg–Ar calibration lamp (HG-2, Ocean Optics, FL, USA). The 520.89 cm^{-1} band of the Si substrate was used as an internal reference. Raman mapping along with nanochannel formation were conducted with a stepper-motor driven *xy* stage (Scanning stage, SCAN 75 × 50, Marzhauser Wetzlar, Germany) and a 1 μm step size was utilized for raster scanning of the sample (raster scanning of the sample with scanning repeatability <1 μm). Raster-scanning Raman mapping, using a coverslip-tolerant objective (LMPlanFI, 50×, NA = 0.50), was conducted for 2, 4, 7, 17, 24, 42, 53, 63, and 75 d periods and the results were collected using a 7 s integration time.

2.4. Nanoballoon formation

After water entrapment was confirmed by Raman spectroscopy, nanoballoons were formed by using irradiation from a higher power laser (50 mW) with a 7 s integration time. Each step size for raster scanning during laser irradiation was 0.5 μm. Laser irradiation on sample was masked every other step. G and 2D bands of SLG were deconvoluted by single Lorentzian fitting, and 2D band of BLG was fitted by four Lorentzian shapes. Especially, component of second lowest frequency were chosen for ω2D of BLG. For Raman mapping, we have collected Raman spectra from 50 different spots and obtained average and standard deviations.

3. Results and discussion

The process developed in this effort for graphene nanostructure formation is illustrated in Fig. 1. In this effort, we found that water diffuses into and forms a sandwiched structure in the interplanar space between graphene and a hydrophobically functionalized SiO_2/Si substrate, and is evaporated and induces formation of graphene nanostructures such as nanochannels and balloons. In present approach, O_2 plasma treated 285 nm thick SiO_2/Si substrate is initially treated with octadecyl-trichlorosilane (OTS) to prepare octadecyl-terminated substrate (ODS) (Fig. 1a, see Experimental for the details). In next step, the graphene sample is prepared by micromechanical exfoliation of a kish graphite flake using Scotch tape onto the substrate (see Experimental). In order to enhance the graphene-substrate interaction [40], the exfoliated graphene sample on the substrate was annealed at 120 °C under vacuum (Fig. 1b). Subsequently, the sample is immersed in a deionized (DI) water contained in a sealed chamber to enable water diffusion into the interplanar space between the graphene and ODS layer (Fig. 1c). Finally, the graphene-water-ODS sample is irradiated with a focused laser (532 nm) of *ca.* 1 μm beam diameter through a coverslip of transparent sample chamber using coverslip-tolerant objective lens. Local heat resulting from the focused laser irradiation is absorbed by the Si substrate and transferred to interfacial water to promote vaporization (Fig. 1d). Owing to the excellent mechanical [7] and hermetic [41] properties of graphene, the water vapor causes graphene to bulge upwards by sliding without tearing.

3.1. Characterization of graphene nanochannels

Studies were conducted to assess the controlled nanochannel formation of graphene occurring on the hydrophobic substrate. The results of contact angle goniometry indicates that ODS has a much higher contact angle θ (*i.e.*, 133.2 ± 1.4°) than those of both bare substrate (*i.e.*, 63.0 ± 2.3°) and O_2 plasma treated substrate (*i.e.*, 14.6 ± 0.8°) (Fig. S2 and inset, see Supporting Information). This observation is in accordance with those reported earlier [38,42], indicating that ODS is successfully produced. The layer number and crystallinity of graphene generated by using micromechanical exfoliation on the substrate were readily determined utilizing optical contrast, atomic force microscopy (AFM), and Raman spectroscopy.

Fig. 2a–b displays AFM topography images of graphene on ODS before and after laser-irradiation to induce vaporization of water entrapped between graphene and ODS. The AFM height topography profile (Fig. 2a) shows that as-exfoliated graphene is composed of different layer numbers that intimately conforms the underlying ODS surface. In order to determine the layer number, a height profile was determined at different locations. The height profile (black trace, Fig. 2c) along segment α displays a 0.53 nm step from the substrate to graphene, which is similar to thickness (0.34 nm) of a single layer of graphene (SLG) [43,44], whereas that the interface between SLG and bilayer of graphene (BLG) displays a 0.38 nm step (Fig. 2a). Further investigation of corresponding AFM phase images (Figs. S3a and b) shows that the interface between SLG and BLG does not show significant phase difference, suggesting

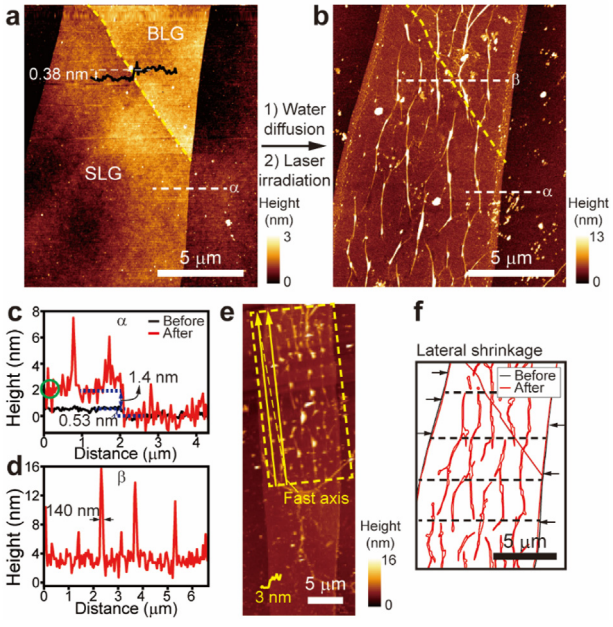

Fig. 2. AFM topography measurements of graphene nanochannels formed by laser-induced vaporization of entrapped water. Height images in (a) as-exfoliated graphene, and (b) laser irradiation of graphene/ODS containing entrapped water. Height profiles in (c) the SLG part along segments α in (a) and (b) before (black) and after laser-irradiation, and (d) SLG and BLG interfaces along segment β in (b). (e) Entire AFM topography of laser irradiated (top) and bare (bottom) regions. Laser-induced nanochannels were formed within exposed area in yellow dashed box in which solid and dashed lines indicate fast and slow axes of laser irradiation direction by raster scanning of *xy* stage. (f) Graphene edge retreatment before (black) and after (red) laser irradiation by overlapping traced edges and nanochannels in (a) and (b). Dashed line is segmentation induced by raster scanning of *xy* stage. (A colour version of this figure can be viewed online.)

continuous atop graphene on discontinuous graphene.

Following immersion in water for 10 days ($t_{water} = 10$), the raster scanning method, with a fast axis along the longitudinal direction of graphene (Fig. 2e), was used. A focused continuous laser (532 nm, 0.5 mW, 7 s/pixel) *via* a coverslip-tolerant 50× objective lens was employed to irradiate the sample in a water chamber with coverslip viewport. Inspection of the AFM topography image of Fig. 2b shows that, upon laser irradiation, the graphene surface becomes decorated with an array of approximately 1 μm-spaced vertical wrinkles which are similar to the step size of the slow axis during raster scanning. This result is in stark contrast with random wrinkles of graphene created by natural drying (see AFM height image and profile of Figs. S4a and b). As can be seen by viewing Fig. 2c and d, the heights of wrinkles created on the graphene surface vary from 4 to 16 nm, and the wrinkles display full width at half maximum height (FWHM) of as large as *ca.* 140 nm with uncertainty originating from 6 nm tip radius of curvature of AFM cantilever. It is noteworthy that wrinkle propagations from SLG and BLG does not produce significant changes in their topographies. Moreover, the graphene surface after water immersion followed by laser irradiation is elevated by 1.4 nm as compared to that of the as-exfoliated material (Fig. 2c). The height difference before and after exposure to water and laser irradiation suggests that the graphene has entrapped water underneath. In addition, the height of the laser irradiated area is slightly less than that (*i.e.*, 3 nm) of the water-entrapped non-irradiated area (Fig. 2e), presumably because water loss has taken place through vaporization. In addition, non-irradiated water-containing graphene does not exhibit a noticeable wrinkle structure. Thus, wrinkle formation clearly results from laser irradiation. In addition, ODS does not show any topographical change (see Experimental), suggesting that water is the main reason for this formation. Upon careful investigation of graphene nanochannel, a series of abrupt changes along wrinkles was observed as indicated by dashed line in Fig. 2f. Those changes seem to originate from the repeatability limitation of motorized *xy* stage (see Experimental). Furthermore, a comparison of the traces before and after the laser irradiation shows that wrinkle formation results in a slight lateral shrinkage (*i.e.*, 70 nm) of graphene edges (Fig. 2f). The length attenuation is a compensation for wrinkle formation, which is in line with graphene shrinkage expected to take place upon formation of graphene nanochannels. In addition, as compared to that before irradiation (black trace of Fig. 2c), the surface profile after laser irradiation (red) shows that some contacts exist between graphene and the bottom ODS substrate (see circled area of Fig. 2c). This result suggests that local pinning of graphene on ODS provides positional stability of graphene during channel formation. Notably, many graphene flakes (Fig. S5) are scrolled during water diffusion due to thermodynamic stability of scrolled form [25,45,46].

A question considering the mechanism of nanochannel formation is the nature of the component(s) responsible for light absorption. It is obvious that, water whose absorption edge is near 180 nm, does not absorb light in the visible region. In contrast, Si with a band gap of 1.1 eV and a wafer thickness of 500 μm is likely the major light absorber. SLG, which has a transparency in the visible range of 97.7% [8], is expected to be a minor 532 nm light absorbing component. Heat created by light absorption of both of these materials is transferred to water to promote vaporization that forms graphene nanochannels. It is well known that laser power density of 10^4–10^6 W/cm^2 realizes high local temperatures (100 °C or higher), which were employed to manipulating Au nanoparticles [47,48]. Based on 1 μm beam diameter and 0.5 mW laser power, laser power density is 1.3×10^5 W/cm^2. In case of direct exposure to graphene/ODS without water for short period (up to 30 s), such irradiation does not result in any change (Figs. S1c and d). However, upon prolonged 50 mW exposure up to few min, graphene forms holes (Figs. S1e and f), suggesting that laser dosage matters. After the vaporization, water would condense into liquid water back due to the graphene pressure which will be discussed later. The 140 nm lateral dimension of the nanochannel, revealed in the AFM measurement, suggests that the heat generated is highly localized and is smaller than 1 μm focused beam size. The localization substantiates the proposal that Si is the major light absorber because it and SiO_2 have much smaller thermal conductivities of 156 and 1.3 W/m•K, respectively [49,50], as compared to that of suspended graphene (4800–5300 W/m•K) [51].

Water trapped between equally hydrophobic planes has somewhat different properties than interfacial water present between graphene and hydrophilic substrates such as mica and SiO_2 [32,52,53]. Xu and coworkers [32] reported that interfacial water in graphene-water-hydrophilic mica has a two water layer thickness (*i.e.*, 0.37 nm), and that is introduced into the interfacial gap between graphene and hydrophilic SiO_2/Si substrate by diffusion [53]. The prolonged stability of its structure in this environment [53] suggests that interfacial water is not fluid but rather it exists as a rigid ice-like layer that holds graphene in place through van der Waals (vdW) interactions. In addition, laser irradiation of the sandwiched structure on a hydrophilic substrate under analogous laser irradiation conditions during focused laser Raman mapping does not result in graphene wrinkle formation [53]. It might be possible to pattern such structure with increased laser dosage which is a topic for future publication. Nevertheless, we speculate that the few tens of layered water molecules entrapped between the hydrophobic graphene and ODS planes is thick enough to enable water to behave like a fluid and decouple vdW interactions (or friction) between the graphene/ODS layers. The graphene on the fluidic water can slide, so the pressure caused by the formed water vapor under laser irradiation results in the movement of graphene, leading to the lateral reduction, and it undergoes bulging-up under the pressure exerted by the formed water vapor.

3.2. Raman spectroscopy investigation of water diffusion into hydrophobic planes

Insight into the diffusion of water between the hydrophobic graphene and ODS layers was gained by using *in situ* Raman spectroscopy and mappings, which is powerful tool to decipher graphene doping and strain in two dimension [54,55]. In Fig. 3a is displayed an optical microscope (OM) image of graphene, showing the optical contrast difference for SLG and BLG domains. Using the aforementioned water chamber with a coverslip, a series of Raman maps were recorded as a function of t_{water} (bottom panel of Fig. 3c–g). Exfoliated graphene on substrate was initially annealed at 120 °C for 10 min to induce an enhancement of the vdW interaction between graphene and substrate [56]. Annealing results in graphene doping and biaxial strain due to the presence of a charge impurity and undulations of the substrate (*i.e.*, 0.19 and 0.2 nm root mean square (rms) roughness for ODS and bare substrates, Figs. S6a and b) [39,56]. The Raman spectrum of the SLG domain (Fig. 3b) contains two prominent peaks at 1586 and 2681 cm^{-1}, corresponding to graphitic G and its overtone 2D bands, respectively [54]. The annealing step results in 5 and 14 cm^{-1} shifts of the positions of the G and 2D bands (ω_G and ω_{2D}, respectively) to higher frequencies than the charge neutral positions *O* ($\omega_G^0 = 1581$ and $\omega_{2D}^0 = 2667$ cm^{-1}, respectively) which are obtained from a spectrum of suspended graphene that is not interacting with substrate [57]. In addition, an appreciable disorder-derived D band near 1345 cm^{-1}, which is typically associated with less fluidic water entrapped between graphene and hydrophilic water, is not observed in the Raman spectrum [53]. The intensity ratio of the 2D

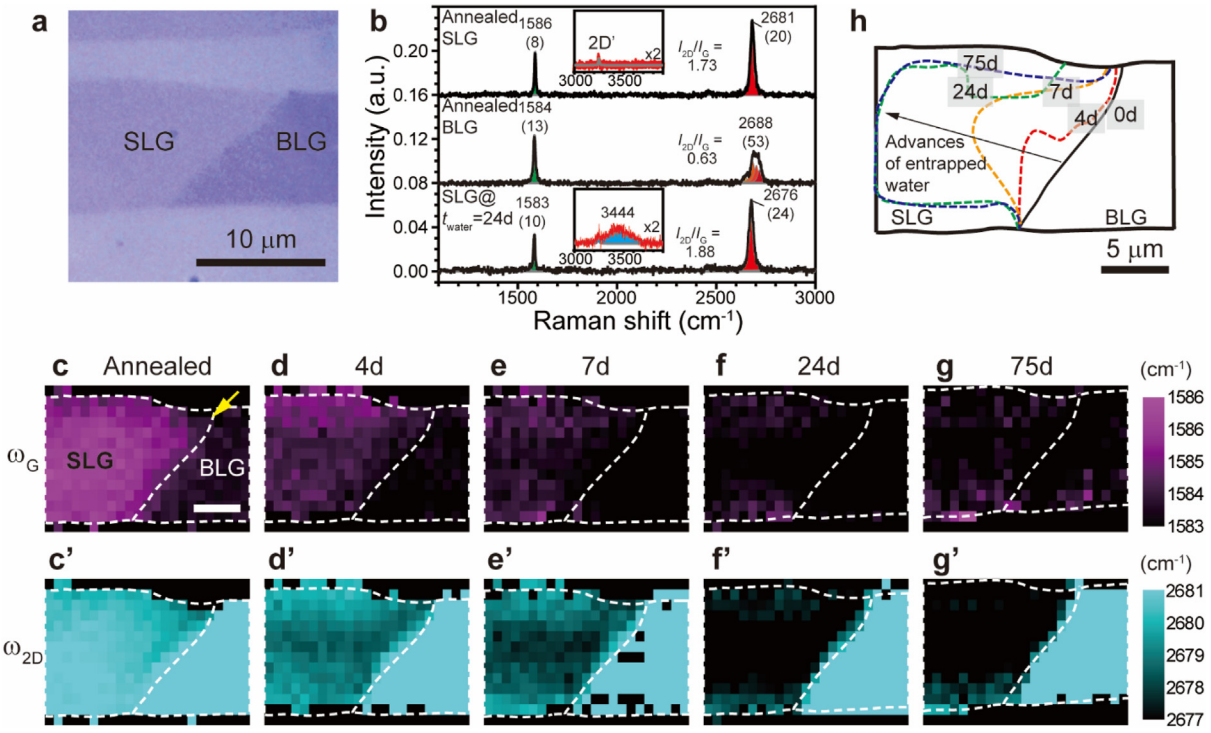

Fig. 3. Raman spectroscopy characterization of water diffusion behavior into the interspace between graphene and ODS. (a) OM image of mechanically exfoliated graphene. (b) Raman spectra of annealed SLG region (top), annealed BLG region (middle) and water-incubated SLG (bottom) after 24 d. Insets show Raman spectra containing water OH bands near 3450 cm^{-1}. (c–g) ω_G maps from annealed and immersed states as a function of t_{water} (*i.e.*, 4, 7, 24 and 75 d). (c'-g') The corresponding ω_{2D} maps. Laser excitation: 532 nm. Scale bar: 5 μm. (h) The advance of entrapped water as a function of t_{water} based on the nearly charge-neutral G band at *ca.* 1583.5 cm^{-1}.

and G bands (I_{2D}/I_G), which is useful for determining layer number [54], is *ca.* 1.7, and FWHM of the 2D band (Γ_{2D}), which is sensitive to layer number, is *ca.* 20 cm^{-1}, a value that is in reasonable agreement with that for SLG (24 cm^{-1}) [54]. Likewise, the BLG region of the spectrum contains G and 2D bands at 1584 and 2688 cm^{-1}, the latter of which can be further deconvoluted into four Lorentzian fits (gray line) which originate from two intervalley phonons scatterings from highly symmetric *K* and *K'* points in the Brillouin zone [58].

Water entrapment causes decoupling of the graphene-substrate interaction and an associated progressive shifts of ω_G and ω_{2D} toward the lower frequencies, showing approaches to the charge-neutral positions *O* [56]. Inspection of the Raman spectrum acquired on the t_{water} = 24 d sample (bottom panel of Fig. 3b) shows that ω_G and ω_{2D} are downshifted respectively by 3 and 5 cm^{-1}, and that Γ_G and Γ_{2D} are broadened (see numbers in bracket) as compared to those bands in the spectrum of the annealed graphene sample. This behavior mainly originates from phonon softening in the G and 2D bands due to de-doping of the Dirac cone of the graphene electronic structure [39,54,56]. Upon closer inspection, we also observed a broad band near 3444 cm^{-1} (see bottom-inset of Fig. 3b), which originates from diffused water along with the 2D' band at 3249 cm^{-1}. This result indicates that water diffuses into the hydrophobic planes.

A series of Raman maps, which are based on trends seen in the positions of ω_G (Fig. 3c–g) and ω_{2D} trends (Fig. 3c'-g') along with their widths (Figs. S7A–E and S7A′-E′ for Γ_G and Γ_{2D} map changes, respectively), were recorded to evaluate how water diffusion occurs in the layer between equally hydrophobic planar structures. As judged by the lower frequency shifts and peak broadening of ω_G and ω_{2D}, water diffusion begins at the interfacial corner of BLG to SLG (yellow arrow in Fig. 3c). This observation indicates that anisotropic water diffusion occurs into the graphene slap where it interacts with ODS to a lesser extent (Fig. S8). Time-dependent water-front advance area, defined by ω_G < 1584 cm^{-1}, is illustrated in Fig. 3h. Diffusion starts at the weakly interacting interfacial corner point and advances to near the central basal plane over few tens of days. The diffusion rate τ of the fastest part of the water-front is *ca.* 2.72 μm/d, and τ becomes slower with t_{water}.

The observed nature of anisotropic and slow water diffusion in between graphene and a hydrophobic substrate is somewhat different from the case of its diffusion in graphene on a bare (hydrophilic) Si substrate [53]. In the latter case, water diffusion occurs on all peripheries of a graphene flake and its rate (2.4–72 μm/d) [53] is 2–26 times faster than that between graphene and a hydrophobic substrate. This finding starkly contrast with the results of recent theoretical calculations that show water diffuses much faster on a hydrophobic surface than it does on a hydrophilic counterpart [59,60]. We speculate the observation of slow water diffusion in hydrophobic planes originates from the vdW interaction occurring between graphene and the hydrophobic substrate. The reason for this mainly stems from the large pressure (*i.e.*, 1 GPa) exerted by the vdW interaction between two graphene sheets [61]. In contrast, carbon nanotube possess cylindrical structure rigidity, display much higher τ than mesoporous silica with a similar pore size [62]. Thus, the vdW pressure plays a key role for water to diffuse into equally hydrophobic surfaces, a conclusion that is in full accord with the observed anisotropic diffusion of water along the weak interaction position with graphene-ODS.

Raman spectroscopic changes taking place with increasing t_{water} were also evaluated. By inspecting the t_{water}-dependent changes of SLG displayed in Fig. 4a. It can be seen that as t_{water} increases ω_G and ω_{2D} progressively shift to lower frequencies and undergo peak broadening. No D peak near 1345 cm^{-1} was observed throughout, which suggests that lattice deformation of graphene on water/hydrophobic substrate does not occur unlike the case from

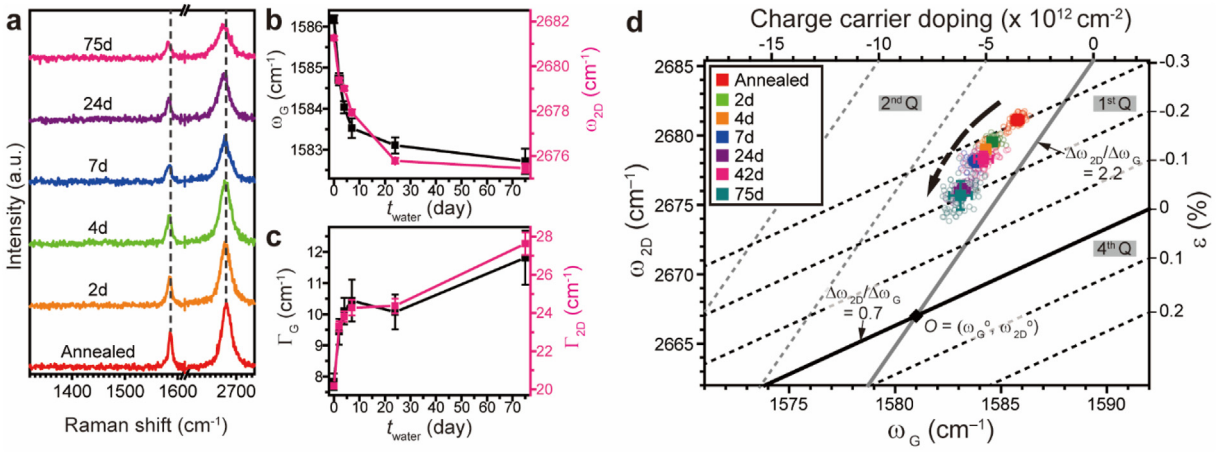

Fig. 4. (a) Raman spectroscopy monitoring of t_{water}-dependent changes of the SLG domain. (b) ω_G and ω_{2D} changes, and (c) Γ_G and Γ_{2D} changes according to t_{water}. (d) Analysis of ω_G and ω_{2D} of graphene for ε and charge carrier doping contributions during water diffusion. Error bars for ω_G and ω_{2D} indicate standard deviations for t_{water}. Diamond represents charge-neutral point O = (1581 and 2667 cm^{-1}). Bold black and gray lines indicate doping- and ε-induced changes of graphene from O. Each dash line indicates ε and doping levels. Note that each quadrant Q is labeled. (A colour version of this figure can be viewed online.)

hydrophilic substrate [53]. This finding indicates that graphene suspended on the entrapped water layer is in a highly uniform environment free from localized strain caused by the underlying topography [53]. Evaluation of the t_{water} dependencies of ω_G and ω_{2D} change (Fig. 4b) shows that these bands undergo exponential low frequency shifts that plateau at 1582 and 2675 cm^{-1}, respectively. In Fig. 4c is displayed the t_{water} dependent peak width behavior of the G and 2D bands. Clearly, peak broadening occurs in concert with a low frequency peak shift as t_{water} increases. Especially interesting is that the respective Γ_G and Γ_{2D} at t_{water} = 75 d are 11.8 and 27.6 cm^{-1}, extreme peak broadening that suggests the occurrence of phonon softening of graphene owing to propensity to charge neutral graphene upon water contact [63,64]. Similar low frequency shifts and broadening behavior were observed to lesser extent in the BLG region (Figs. S9a–c).

It is known that water intercalation affects strain and doping of graphene. Studies have shown that ω_G and ω_{2D} display quasi-linear responses to levels of graphene doping [63] and biaxial strain (ε) [65]. Lee and coworkers [66] reported that the crossing point of ω_G and ω_{2D} can be dissected into doping and biaxial ε contributions [66]. According to this method and the one we developed previously [39], the t_{water} dependent behavior of ω_G and ω_{2D} was evaluated in terms of doping and ε contributions. In Fig. 4d is given a plot of ω_G *vs* ω_{2D} trends dissected into charge carrier doping and strain components. The respective bottom and top abscissas denote ω_G and concomitant charge doping level (*i.e.*, positive and negative signs denote *p*- and *n*-doping, respectively). The left and right ordinates denote ω_{2D} and biaxial ε (*i.e.*, positive and negative signs denote respective tensile and compressive ε). Changes in ε (*i.e.*, $\Delta\omega_{2D}/\Delta\omega_G = 2.2$) and doping ($\Delta\omega_{2D}/\Delta\omega_G = 0.7$), originating from the biaxial strain and doping responses of SLG [66], are indicated in bold lines. The Raman map of annealed graphene on ODS displays average ω_G and ω_{2D} of 1586.0 ± 0.3 and 2681.4 ± 0.4 cm^{-1} (Table S1) with respect to positions of charge neutral graphene O (1581 and 2667 cm^{-1}, respectively). The Raman positions of the annealed graphene display 0.3% compressive ε with slight *n*-doping with respect to charge neutral values. The spread of ω_G and ω_{2D} in graphene on the hydrophobic state as indicated by error bars is approximately four times narrower than that (*i.e.*, ±1.2, ±1.7) of graphene on a hydrophilic substrate annealed at a similar temperature (*i.e.*, 100 °C) [66]. Importantly, a comparison of the ω_{2D} spread in materials with hydrophobic and hydrophilic substrates indicates that ODS provides a more uniform charge and ε distribution along the surface, and subsequently provides less localized compressive ε, which is in accordance with earlier observations [38]. As t_{water} increases, ω_G and ω_{2D} progressively shift to lower frequencies mainly along the ε axis. This result suggests that compressive ε is slowly relieved from graphene on substrate and approaches the charge neural value when water diffuses between the graphene and ODS. This result suggests that graphene can be utilized as sensitive indicator for water intercalation and substrate interactions in hydrophobic substrates.

3.3. Formation and characterization of graphene nanoballoon

A further effort demonstrated that by using a similar approach using programmed laser irradiation, a graphene nanoballoon structure can be created. For this purpose, irradiation of water incubated graphene-ODS was conducted using 0.5 μm stepsized alternative masking of continuous laser irradiation (*i.e.*, 50 mW). AFM topography showed that while as prepared graphene-ODS (Fig. 5a) contains a clean graphene surface, material obtained by using programmed laser irradiation (Fig. 5b) contains 1 μm spaced, not spherical but slightly elongated nanoballoon structures. It is noteworthy that appreciable D band increase was not observed as compared to bare positions even after 50 mW laser irradiation on graphene in water-containing chamber (Figs. S10a–e), judged by intensity ratios of D over G bands from several positions (*i.e.*, 0.13 ± 0.02 vs 0.11 ± 0.01 for laser-irradiated and bare positions, respectively). This seems to originate from the chemical inertness of graphene against water upon laser irradiation. The nanoballoon structure (Fig. 5c) is retained even after 4 months, but the heights of the nanoballoons decrease from 12 nm to 4 nm (Fig. 5d). Because graphene has elastic properties, nonlinear plate theory was utilized to calculate the adhesion energy (E) and pressure (P) of the nanoballoon (see SI for the detailed explanation) [67]. Heights and radius data collected from five nanoballoons (Figs. S11a–e) were used to show that P varies from 0.18 to 0.43 MPa (Table S2), indicating that the pressure in the nanoballoon is slightly higher than atmospheric pressure, supporting slightly irregular circular shape of nanoballoon. P from 4 month old sample approaches to *ca.* 0.1 MPa, atmospheric pressure. In addition, E was shown 0.55–2.6 mJ/m^2, suggesting that E of graphene on entrapped water/hydrophobic substrate is quite small, much smaller than those of graphene on Cu (*i.e.*, 12.8 J/m^2) [68] and on hydrophobic poly(-dimethylsiloxane) (*i.e.*, 7 mJ/m^2) [69]. It should be noted that the

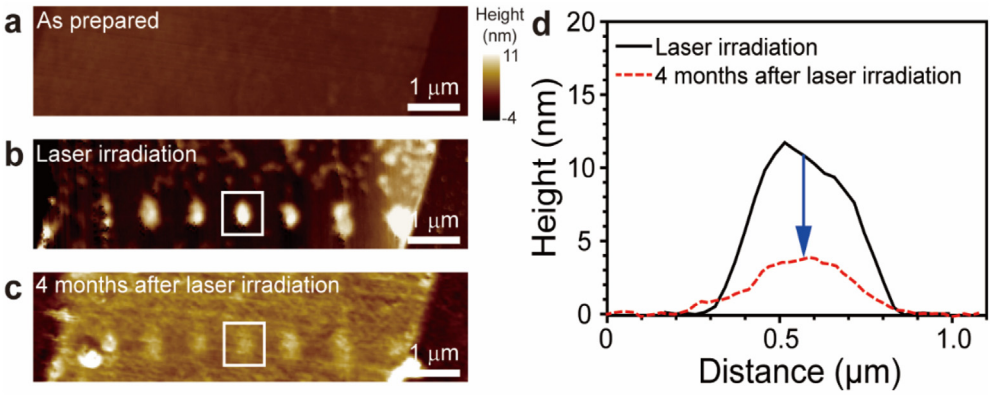

Fig. 5. Graphene nanoballoon formation by programmed laser irradiation. AFM topographies of (a) as prepared graphene on ODS, (b) programmed on/off laser irradiated graphene on ODS after water entrapment, and (c) 4 months after laser irradiation. (d) Height profiles of graphene immediately after laser irradiation (solid line) and 4 months after laser irradiation (dashed line) from rectangles of (b) and (c).

results of theoretical calculations show that graphene on SiO_2 surface has lower adhesion energy when SiO_2 surface is either hydroxylated or water is adsorbed [70]. Experimental results arising in this investigation along with previously reported observations suggest that graphene on water exerts an extremely small *E* with underlying substrate, which facilitates nanostructure formation of graphene by enabling ready sliding and bulging. Additionally, those graphene nanoballoons created in similar manners can be observed by scanning electron microscopy (SEM) image as demonstrated in Figs. S12a and b.

By comparing nanochannel and nanoballoon cases, the created nanochannel and nanoballoon have similar order of FWHM (*i.e.*, 140 nm *vs* 260 nm, respectively) despite large difference in the used laser intensities (0.5 *vs* 50 mW, respectively). Consideration of 100 times large intensity cannot give similar order of FWHM. This directs to consider the role of limited amount of water for the shaping of nanostructures. Since entrapped water was finite amount (*i.e.*, 1.4–3.0 nm in height), those seem to serve as a limiting factor for shaping the graphene nanostructures. Behind the graphene nanostructure formation, water fluidity plays important roles for the process of formation of graphene nanostructures. Fluidic water rather than ice-like water facilitates graphene sliding motion as evident by lateral shrinkage of the laser-irradiated graphene. In addition, fluidic water slowly relieved graphene strain which is induced by graphene/substrate interaction. Lastly, the aforementioned vdW interaction between graphene and hydrophobic substrate would further prompt for possible ice water to melt. Those aspects are important to explain the formation of graphene nanostructure.

4. Conclusions

In the investigation described above, we demonstrated that focused laser irradiation of a graphene-water-hydrophobic substrate can be utilized to form graphene nanostructures including nanochannel and nanoballoon. In the process, the focused laser beam irradiation promotes vaporization of confined water which causes the mechanically robust graphene to bulge upwards by sliding on the water surface by virtue of vdW interaction between the equally hydrophobic slap. Water is slowly and anisotopically diffused into hydrophobically interplanar space. Interplanar water diffusion decouples the graphene-substrate interaction and progressively leads to production of charge-neutral graphene as the immersion time increases by using Raman spectroscopy and time-lapsed mapping. These observations were employed to create graphene nanoballoons. Along with detailed understanding of water diffusion in between hydrophobic graphene/substrate, these observations open a new strategy to construct morphologically modified graphenes and other related two-dimensional materials which are useful in fundamental studies and for applications to various nanofluidic devices such as those utilized for bio-sensing, ion transport and water filtration.

CRediT authorship contribution statement

Sukhyun Hong: Prepared samples and performed characterizations. **Minsuk Park:** Performed AFM and Raman characterizations. **Soonhyung Kwon:** Prepared samples and performed characterizations. **Jehyun Oh:** Performed AFM and Raman characterizations. **Sungmin Bong:** performed AFM and Raman characterizations. **Balu Krishnakumar:** read and corrected the manuscript. **Sang-Yong Ju:** Conceived the idea and wrote the manuscript.

Declaration of competing interest

The authors declare that they have no known competing financial interests or personal relationships that could have appeared to influence the work reported in this paper.

Acknowledgments

The authors acknowledged H.K., and E.K. for initial help. This research was mainly financially supported by the Basic Science Research Program through the National Research Foundation of Korea (NRF) funded by the Ministry of Education, Science, and Technology (2020R1F1A107698311, 2020R1A4A101773711, and in part 2019R1A6A3A13091240). B.K. thanks award from Yonsei Frontier Program for Young Postdoctoral Researchers 2020.

Appendix A. Supplementary data

Supplementary data to this article can be found online at https://doi.org/10.1016/j.carbon.2021.06.071.

References

[1] R. Karnik, R. Fan, M. Yue, D. Li, P. Yang, A. Majumdar, Electrostatic control of ions and molecules in nanofluidic transistors, Nano Lett. 5 (5) (2005) 943–948.
[2] S.W.P. Turner, M. Cabodi, H.G. Craighead, Confinement-induced entropic recoil of single DNA molecules in a nanofluidic structure, Phys. Rev. Lett. 88 (12) (2002), 128103.

[3] C. Danelon, C. Santschi, J. Brugger, H. Vogel, Fabrication and functionalization of nanochannels by electron-beam-induced silicon oxide deposition, Langmuir 22 (25) (2006) 10711–10715.
[4] D.W. Inglis, E.M. Goldys, N.P. Calander, Simultaneous concentration and separation of proteins in a nanochannel, Angew. Chem. Int. Ed. 50 (33) (2011) 7546–7550.
[5] W.-L. Hsu, D.J.E. Harvie, M.R. Davidson, H. Jeong, E.M. Goldys, D.W. Inglis, Concentration gradient focusing and separation in a silica nanofluidic channel with a non-uniform electroosmotic flow, Lab Chip 14 (18) (2014) 3539–3549.
[6] H. Cao, J.O. Tegenfeldt, R.H. Austin, S.Y. Chou, Gradient nanostructures for interfacing microfluidics and nanofluidics, Appl. Phys. Lett. 81 (16) (2002) 3058–3060.
[7] C. Lee, X. Wei, J.W. Kysar, J. Hone, Measurement of the elastic properties and intrinsic strength of monolayer graphene, Science 321 (5887) (2008) 385–388.
[8] R.R. Nair, P. Blake, A.N. Grigorenko, K.S. Novoselov, T.J. Booth, T. Stauber, et al., Fine structure constant defines visual transparency of graphene, Science 320 (5881) (2008) 1308.
[9] K.S. Kim, Y. Zhao, H. Jang, S.Y. Lee, J.M. Kim, K.S. Kim, et al., Large-scale pattern growth of graphene films for stretchable transparent electrodes, Nature 457 (7230) (2009) 706–710.
[10] S. Bae, H. Kim, Y. Lee, X. Xu, J.-S. Park, Y. Zheng, et al., Roll-to-roll production of 30-inch graphene films for transparent electrodes, Nat. Nanotechnol. 5 (8) (2010) 574–578.
[11] M. Majumder, N. Chopra, R. Andrews, B.J. Hinds, Nanoscale hydrodynamics: enhanced flow in carbon nanotubes, Nature 438 (7064) (2005) 44.
[12] J.K. Holt, H.G. Park, Y. Wang, M. Stadermann, A.B. Artyukhin, C.P. Grigoropoulos, et al., Fast mass transport through sub-2-nanometer carbon nanotubes, Science 312 (5776) (2006) 1034–1037.
[13] P. Pang, J. He, J.H. Park, P.S. Krstić, S. Lindsay, Origin of giant ionic currents in carbon nanotube channels, ACS Nano 5 (9) (2011) 7277–7283.
[14] H. Huang, Z. Song, N. Wei, L. Shi, Y. Mao, Y. Ying, et al., Ultrafast viscous water flow through nanostrand-channelled graphene oxide membranes, Nat. Commun. 4 (2013) 2979.
[15] P. Sun, H. Liu, K. Wang, M. Zhong, D. Wu, H. Zhu, Ultrafast liquid water transport through graphene-based nanochannels measured by isotope labelling, Chem. Commun. 51 (15) (2015) 3251–3254.
[16] G.F. Schneider, S.W. Kowalczyk, V.E. Calado, G. Pandraud, H.W. Zandbergen, L.M.K. Vandersypen, et al., DNA translocation through graphene nanopores, Nano Lett. 10 (8) (2010) 3163–3167.
[17] S.T. Martin, A. Neild, M. Majumder, Graphene-based ion rectifier using macroscale geometric asymmetry, APL Mater. 2 (9) (2014), 092803.
[18] R.C. Rollings, A.T. Kuan, J.A. Golovchenko, Ion selectivity of graphene nanopores, Nat. Commun. 7 (2016) 11408.
[19] S. Garaj, W. Hubbard, A. Reina, J. Kong, D. Branton, J.A. Golovchenko, Graphene as a subnanometre trans-electrode membrane, Nature 467 (7312) (2010) 190–193.
[20] W. Xiong, J.Z. Liu, M. Ma, Z. Xu, J. Sheridan, Q. Zheng, Strain engineering water transport in graphene nanochannels, Phys. Rev. E 84 (5) (2011), 056329.
[21] S.K. Min, W.Y. Kim, Y. Cho, K.S. Kim, Fast DNA sequencing with a graphene-based nanochannel device, Nat. Nanotechnol. 6 (3) (2011) 162–165.
[22] J. Liu, L. Cui, D. Losic, Graphene and graphene oxide as new nanocarriers for drug delivery applications, Acta Biomater. 9 (12) (2013) 9243–9257.
[23] L. Feng, L. Wu, X. Qu, New horizons for diagnostics and therapeutic applications of graphene and graphene oxide, Adv. Mater. 25 (2) (2013) 168–186.
[24] Q. Xie, F. Xin, H.G. Park, C. Duan, Ion transport in graphene nanofluidic channels, Nanoscale 8 (47) (2016) 19527–19535.
[25] U. Mirsaidov, V.R.S.S. Mokkapati, D. Bhattacharya, H. Andersen, M. Bosman, B. Ozyilmaz, et al., Scrolling graphene into nanofluidic channels, Lab Chip 13 (15) (2013) 2874–2878.
[26] M.J. Lee, J.S. Choi, J.-S. Kim, I.-S. Byun, D.H. Lee, S. Ryu, et al., Characteristics and effects of diffused water between graphene and a SiO_2 substrate, Nano Res. 5 (10) (2012) 710–717.
[27] T. Verhagen, J. Klimes, B. Pacakova, M. Kalbac, J. Vejpravova, Anomalous freezing of low-dimensional water confined in graphene nanowrinkles, ACS Nano 14 (11) (2020) 15587–15594.
[28] Q. Xie, M.A. Alibakhshi, S. Jiao, Z. Xu, M. Hempel, J. Kong, et al., Fast water transport in graphene nanofluidic channels, Nat. Nanotechnol. 13 (3) (2018) 238–245.
[29] Q. Li, J. Song, F. Besenbacher, M. Dong, Two-dimensional material confined water, Acc. Chem. Res. 48 (1) (2015) 119–127.
[30] P. Bampoulis, K. Sotthewes, E. Dollekamp, B. Poelsema, Water confined in two-dimensions: fundamentals and applications, Surf. Sci. Rep. 73 (6) (2018) 233–264.
[31] Y. Hong, S. Wang, Q. Li, X. Song, Z. Wang, X. Zhang, et al., Interfacial icelike water local doping of graphene, Nanoscale 11 (41) (2019) 19334–19340.
[32] K. Xu, P. Cao, J.R. Heath, Graphene visualizes the first water adlayers on mica at ambient conditions, Science 329 (5996) (2010) 1188–1191.
[33] J. Shim, C.H. Lui, T.Y. Ko, Y.-J. Yu, P. Kim, T.F. Heinz, et al., Water-gated charge doping of graphene induced by mica substrates, Nano Lett. 12 (2) (2012) 648–654.
[34] N. Severin, P. Lange, I.M. Sokolov, J.P. Rabe, Reversible dewetting of a molecularly thin fluid water film in a soft graphene–mica slit pore, Nano Lett. 12 (2) (2012) 774–779.
[35] O. Ochedowski, B.K. Bussmann, M. Schleberger, Graphene on mica-intercalated water trapped for life, Sci. Rep. 4 (1) (2014) 6003.
[36] E. Dollekamp, P. Bampoulis, D.P. Faasen, H.J.W. Zandvliet, E.S. Kooij, Charge induced dynamics of water in a graphene–mica slit pore, Langmuir 33 (43) (2017) 11977–11985.
[37] Y. Huang, E. Sutter, N.N. Shi, J. Zheng, T. Yang, D. Englund, et al., Reliable exfoliation of large-area high-quality flakes of graphene and other two-dimensional materials, ACS Nano 9 (11) (2015) 10612–10620.
[38] Q.H. Wang, Z. Jin, K.K. Kim, A.J. Hilmer, G.L.C. Paulus, C.-J. Shih, et al., Understanding and controlling the substrate effect on graphene electron-transfer chemistry via reactivity imprint lithography, Nat. Chem. 4 (9) (2012) 724–732.
[39] E. Koo, S.-Y. Ju, Role of residual polymer on chemical vapor grown graphene by Raman spectroscopy, Carbon 86 (2015) 318–324.
[40] K.S. Novoselov, A.K. Geim, S.V. Morozov, D. Jiang, Y. Zhang, S.V. Dubonos, et al., Electric field effect in atomically thin carbon films, Science 306 (5696) (2004) 666–669.
[41] J.S. Bunch, S.S. Verbridge, J.S. Alden, A.M. van der Zande, J.M. Parpia, H.G. Craighead, et al., Impermeable atomic membranes from graphene sheets, Nano Lett. 8 (8) (2008) 2458–2462.
[42] Y. Li, C.-Y. Xu, P. Hu, L. Zhen, Carrier control of MoS_2 nanoflakes by functional self-assembled monolayers, ACS Nano 7 (9) (2013) 7795–7804.
[43] W. Bao, K. Myhro, Z. Zhao, Z. Chen, W. Jang, L. Jing, et al., In Situ observation of electrostatic and thermal manipulation of suspended graphene membranes, Nano Lett. 12 (11) (2012) 5470–5474.
[44] E. Koo, S. Kim, S.-Y. Ju, Relationships between the optical and Raman behavior of van Hove singularity in twisted bi- and fewlayer graphenes and environmental effects, Carbon 111 (2017) 238–247.
[45] S.F. Braga, V.R. Coluci, S.B. Legoas, R. Giro, D.S. Galvão, R.H. Baughman, Structure and dynamics of carbon nanoscrolls, Nano Lett. 4 (5) (2004) 881–884.
[46] X. Xie, L. Ju, X. Feng, Y. Sun, R. Zhou, K. Liu, et al., Controlled fabrication of high-quality carbon nanoscrolls from monolayer graphene, Nano Lett. 9 (7) (2009) 2565–2570.
[47] K. Setoura, Y. Okada, S. Hashimoto, CW-laser-induced morphological changes of a single gold nanoparticle on glass: observation of surface evaporation, Phys. Chem. Chem. Phys. 16 (48) (2014) 26938–26945.
[48] K. Setoura, D. Werner, S. Hashimoto, Optical scattering spectral thermometry and refractometry of a single gold nanoparticle under CW laser excitation, J. Phys. Chem. C 116 (29) (2012) 15458–15466.
[49] C.J. Glassbrenner, G.A. Slack, Thermal conductivity of silicon and germanium from 3^{o}K to the melting point, Phys. Rev. 134 (4A) (1964) A1058–A1069.
[50] F.R. Brotzen, P.J. Loos, D.P. Brady, Thermal conductivity of thin SiO_2 films, Thin Solid Films 207 (1) (1992) 197–201.
[51] A.A. Balandin, S. Ghosh, W. Bao, I. Calizo, D. Teweldebrhan, F. Miao, et al., Superior thermal conductivity of single-layer graphene, Nano Lett. 8 (3) (2008) 902–907.
[52] K.T. He, J.D. Wood, G.P. Doidge, E. Pop, J.W. Lyding, Scanning tunneling microscopy study and nanomanipulation of graphene-coated water on mica, Nano Lett. 12 (6) (2012) 2665–2672.
[53] D. Lee, G. Ahn, S. Ryu, Two-dimensional water diffusion at a graphene–silica interface, J. Am. Chem. Soc. 136 (18) (2014) 6634–6642.
[54] L.M. Malard, M.A. Pimenta, G. Dresselhaus, M.S. Dresselhaus, Raman spectroscopy in graphene, Phys. Rep. 473 (5–6) (2009) 51–87.
[55] A.C. Ferrari, D.M. Basko, Raman spectroscopy as a versatile tool for studying the properties of graphene, Nat. Nanotechnol. 8 (4) (2013) 235–246.
[56] S. Ryu, L. Liu, S. Berciaud, Y.-J. Yu, H. Liu, P. Kim, et al., Atmospheric oxygen binding and hole doping in deformed graphene on a SiO_2 substrate, Nano Lett. 10 (12) (2010) 4944–4951.
[57] S. Berciaud, S. Ryu, L.E. Brus, T.F. Heinz, Probing the intrinsic properties of exfoliated graphene: Raman spectroscopy of free-standing monolayers, Nano Lett. 9 (1) (2009) 346–352.
[58] A.C. Ferrari, J.C. Meyer, V. Scardaci, C. Casiraghi, M. Lazzeri, F. Mauri, et al., Raman spectrum of graphene and graphene layers, Phys. Rev. Lett. 97 (18) (2006), 187401.
[59] J.H. Park, N.R. Aluru, Diffusion of water submonolayers on hydrophilic surfaces, Appl. Phys. Lett. 93 (25) (2008).
[60] J.H. Park, N.R. Aluru, Ordering-induced fast diffusion of nanoscale water film on graphene, J. Phys. Chem. C 114 (6) (2010) 2595–2599.
[61] G. Algara-Siller, O. Lehtinen, F.C. Wang, R.R. Nair, U. Kaiser, H.A. Wu, et al., Square ice in graphene nanocapillaries, Nature 519 (7544) (2015) 443–445.
[62] X. Liu, X. Pan, S. Zhang, X. Han, X. Bao, Diffusion of water inside carbon nanotubes studied by pulsed field gradient NMR spectroscopy, Langmuir 30 (27) (2014) 8036–8045.
[63] A. Das, B. Chakraborty, S. Piscanec, S. Pisana, A.K. Sood, A.C. Ferrari, Phonon renormalization in doped bilayer graphene, Phys. Rev. B 79 (15) (2009), 155417.
[64] J. Yan, E.A. Henriksen, P. Kim, A. Pinczuk, Observation of anomalous phonon softening in bilayer graphene, Phys. Rev. Lett. 101 (13) (2008), 136804.
[65] D. Yoon, Y.-W. Son, H. Cheong, Strain-dependent splitting of the double-resonance Raman scattering band in graphene, Phys. Rev. Lett. 106 (15) (2011), 155502.
[66] J.E. Lee, G. Ahn, J. Shim, Y.S. Lee, S. Ryu, Optical separation of mechanical strain from charge doping in graphene, Nat. Commun. 3 (2012) 1024.
[67] H. Ghorbanfekr-Kalashami, K.S. Vasu, R.R. Nair, F.M. Peeters, M. Neek-Amal, Dependence of the shape of graphene nanobubbles on trapped substance, Nat.

Commun. 8 (1) (2017) 15844.
[68] S. Das, D. Lahiri, D.-Y. Lee, A. Agarwal, W. Choi, Measurements of the adhesion energy of graphene to metallic substrates, Carbon 59 (2013) 121–129.
[69] S. Scharfenberg, D.Z. Rocklin, C. Chialvo, R.L. Weaver, P.M. Goldbart, N. Mason, Probing the mechanical properties of graphene using a corrugated elastic substrate, Appl. Phys. Lett. 98 (9) (2011), 091908.
[70] W. Gao, P. Xiao, G. Henkelman, K.M. Liechti, R. Huang, Interfacial adhesion between graphene and silicon dioxide by density functional theory with van der Waals corrections, J. Phys. D 47 (25) (2014), 255301.

Supporting Information

Formation of Graphene Nanostructures using Laser Induced Vaporization of Entrapped Water

*Sukhyun Hong, Minsuk Park, Soonhyung Kwon, Jehyun Oh, Sungmin Bong, Balu Krishnakumar, and Sang-Yong Ju**

Department of Chemistry, Yonsei University, 50 Yonsei-ro, Seodaemun-Gu, Seoul 03722, Korea

* Correspondence E-mail: syju@yonsei.ac.kr

***E* and *P* calculations of nanoballoons.**

The size of a bubble depends on the number of trapped atoms/molecules and the induced hydrostatic pressure inside the bubble is determined by the adhesion forces between the layers forming the nanoballoon. [S1] Using membrane theory for round shaped bubbles, the hydrostatic pressure (*P*) and adhesion energy (*E*) of the graphene bubbles were calculated by using the following equations.[S2, S3]

$$E \cong 1.79\frac{Yh^4}{R^4}$$

$$P \cong 2.85\frac{Yh^3}{R^4}$$

where *Y*, *h*, and *R* are Young's modulus of graphene (340 N/m)[S4], bubble height, and radius of bubble, respectively. In fact, the notable elastic properties of monolayer graphene and the strong interfacial adhesion between graphene and the substrate causes the intercalated atoms to be squeezed into an extremely small volume where they experience a pressure on the order of GPa. Furthermore, nonlinear plate theory can be utilized to modify the above equation to become:

$$E \cong \frac{Yh^4}{R^4} + 32\frac{\kappa h^2}{R^4}$$

$$P \cong 2.56\frac{Yh^3}{R^4} + 64\frac{\kappa h}{R^4}$$

where κ is the bending energy of graphene (0.24 nN·nm). Based on these equations, a graphene nanoballoon having h = 12 nm and R = 250 nm is calculated to have P = 0.265 MPa and E = 1.1 mJ/m^2.

Figure S1. Confirmation of laser-induced damage on ODS in water and graphene/ODS without water by varying focused laser intensity from 0.5 to 65 mW. (a) OM image and (b) corresponding AFM height image after laser irradiation for 30 sec. (c) OM image before laser irradiation, and (d) AFM height image after laser irradiation for 30 sec. (c) OM image before laser irradiation, and (d) AFM height image after laser irradiation for 3 min.

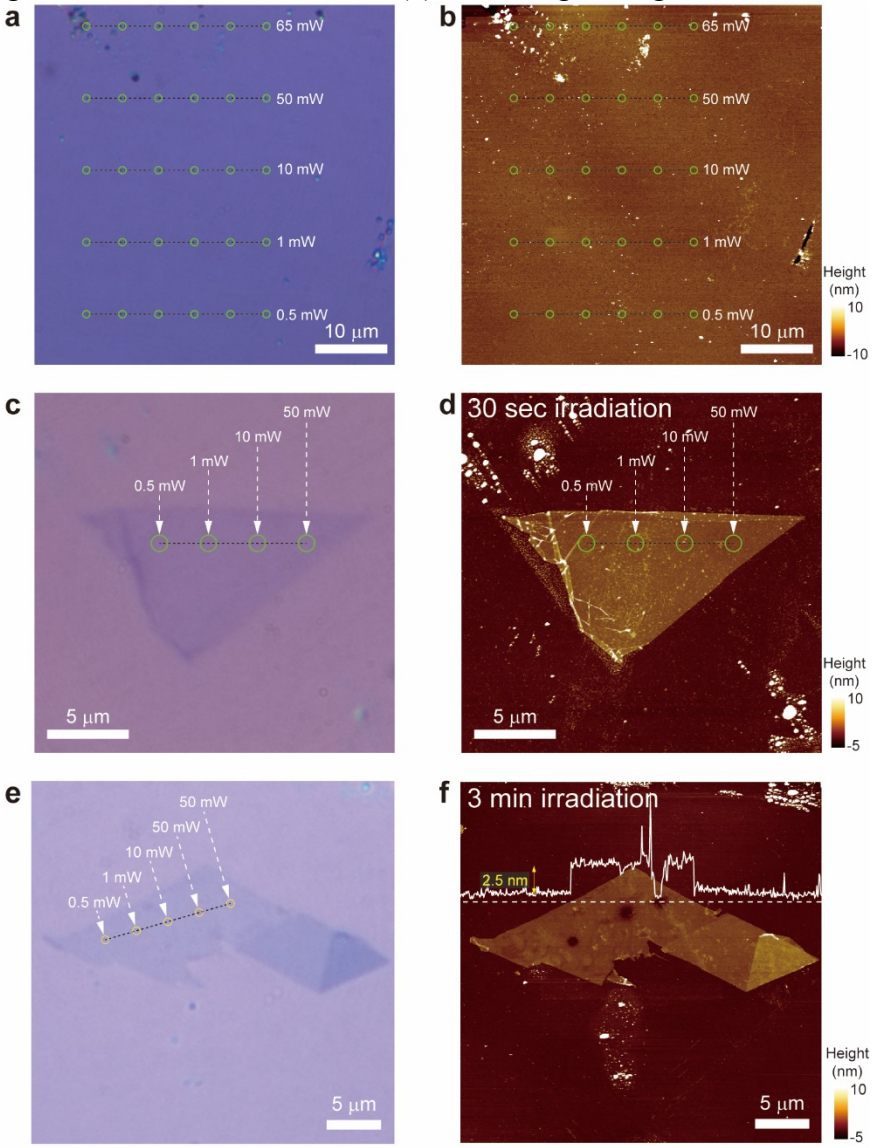

Figure S2. θ measurements of different surface functionalizations.

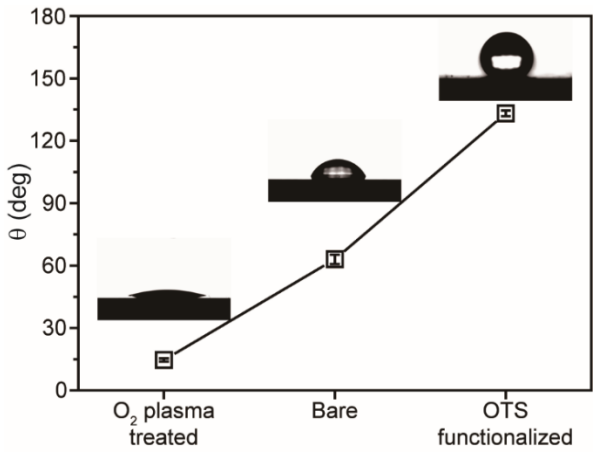

Figure S3. The corresponding phase images of (a) Figure 2a and (b) Figure 2b.

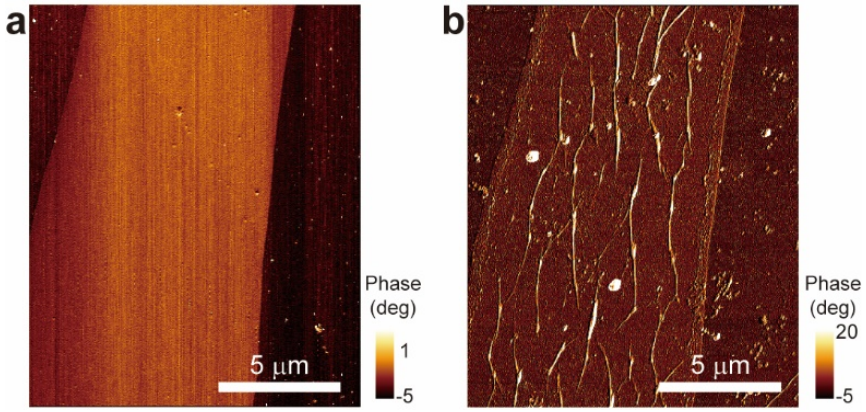

Figure S4. (A) Random wrinkle formations of water-entrapped graphene sample upon natural drying and (B) height profile.

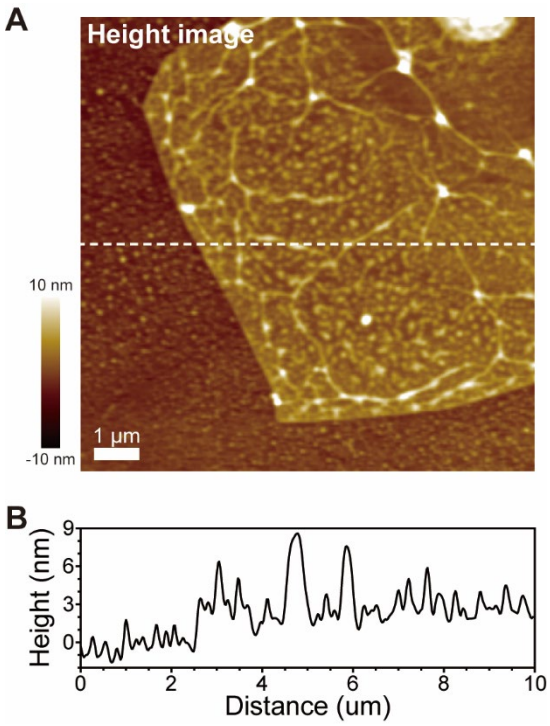

Figure S5. Scrolling of graphenes on ODS during water immersion.

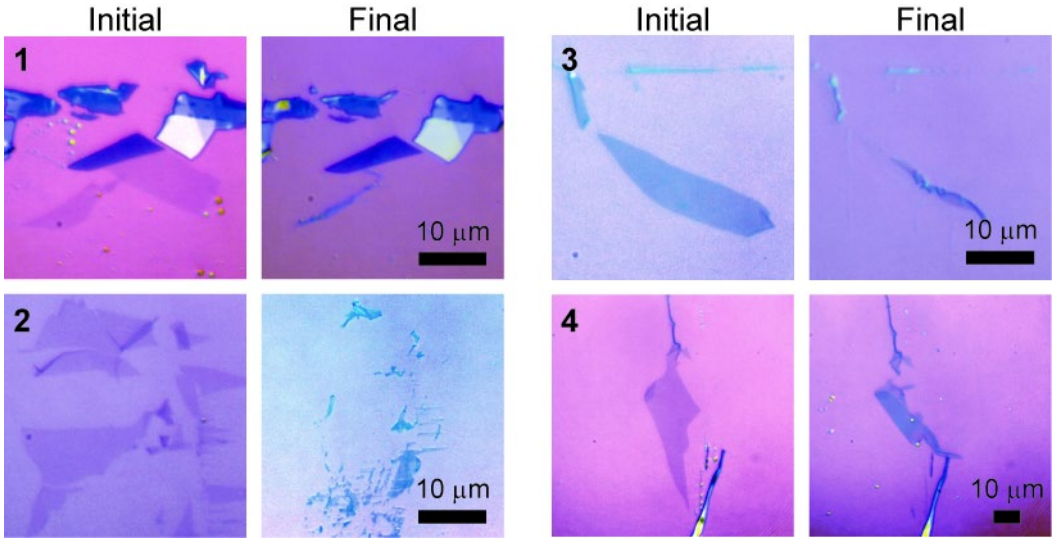

Figure S6. Comparison of RMS roughness of (a) ODS and (b) bare substrates.

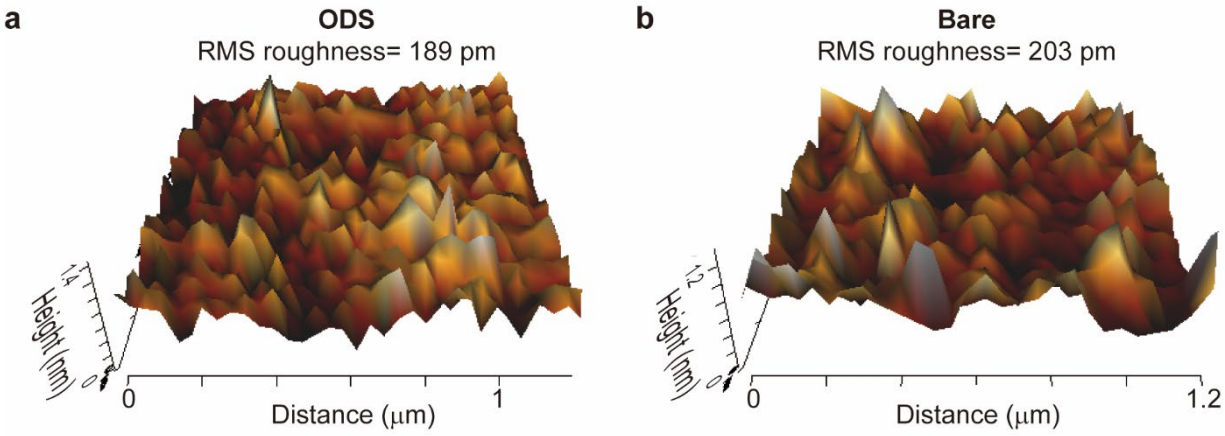

Figure S7. Γ_G and Γ_{2D} map changes of graphene according to t_{water}. (a-e) Γ_G maps from the annealed and immersed states at certain time (*i.e.*, 4d, 7d, 24d, and 75d). (a'-e') The corresponding Γ_{2D} maps. Laser excitation: 532 nm. Scale bar: 5 μm.

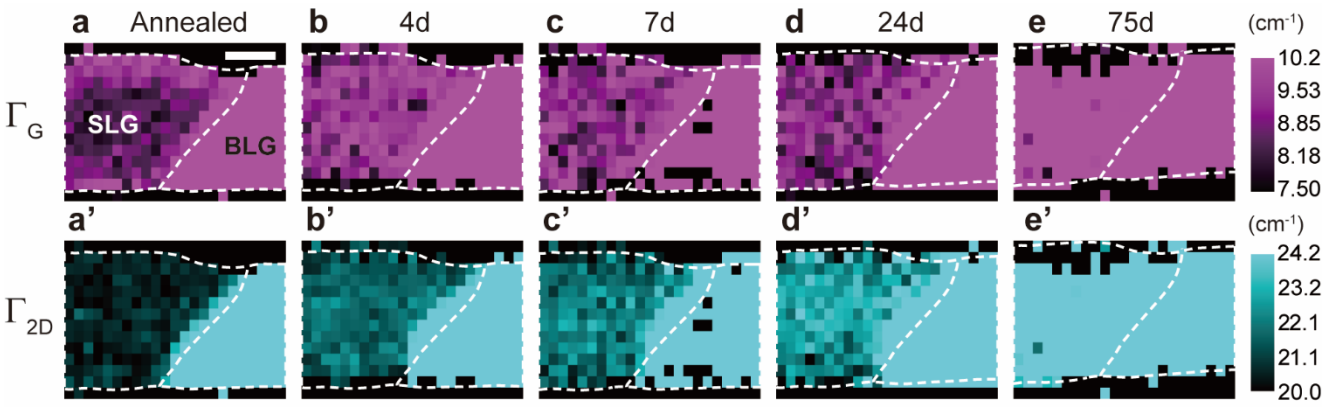

Figure S8. ω_G change of SLG according to regions during water diffusion. Inset shows ω_G map with the positions in which data were collected.

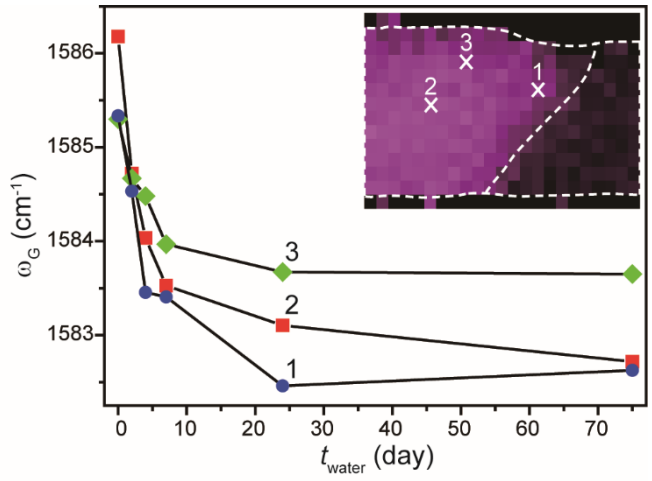

Figure S9. (a) Raman spectral changes of BLG domain according to t_{water}. (b) ω_G and ω_{2D} changes, and (c) Γ_G and Γ_{2D} changes. ω_{2D} was taken from second lowest frequency bands among four Lorentzians.

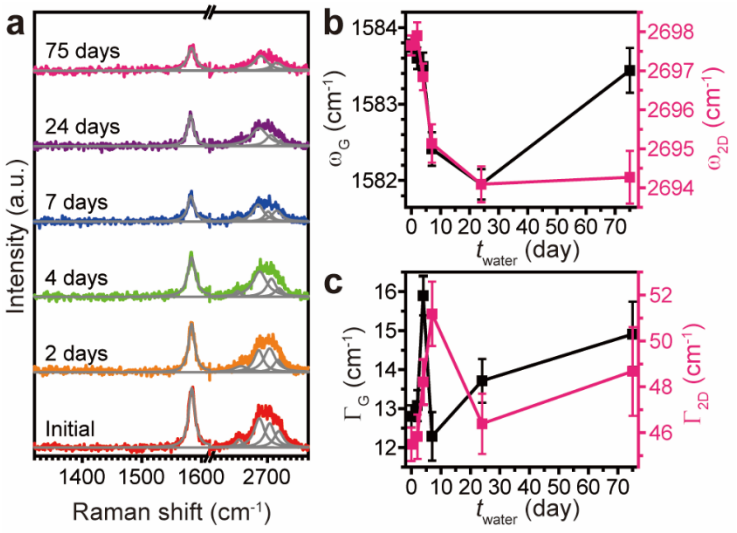

Figure S10. Defect assessment of graphene after the laser irradiation. (a) AFM height image, and the corresponding (b) G band, (c) D band intensity images by Raman mapping of water-entrapped graphene. Offset Raman spectra of (d) α positions and (e) β positions.

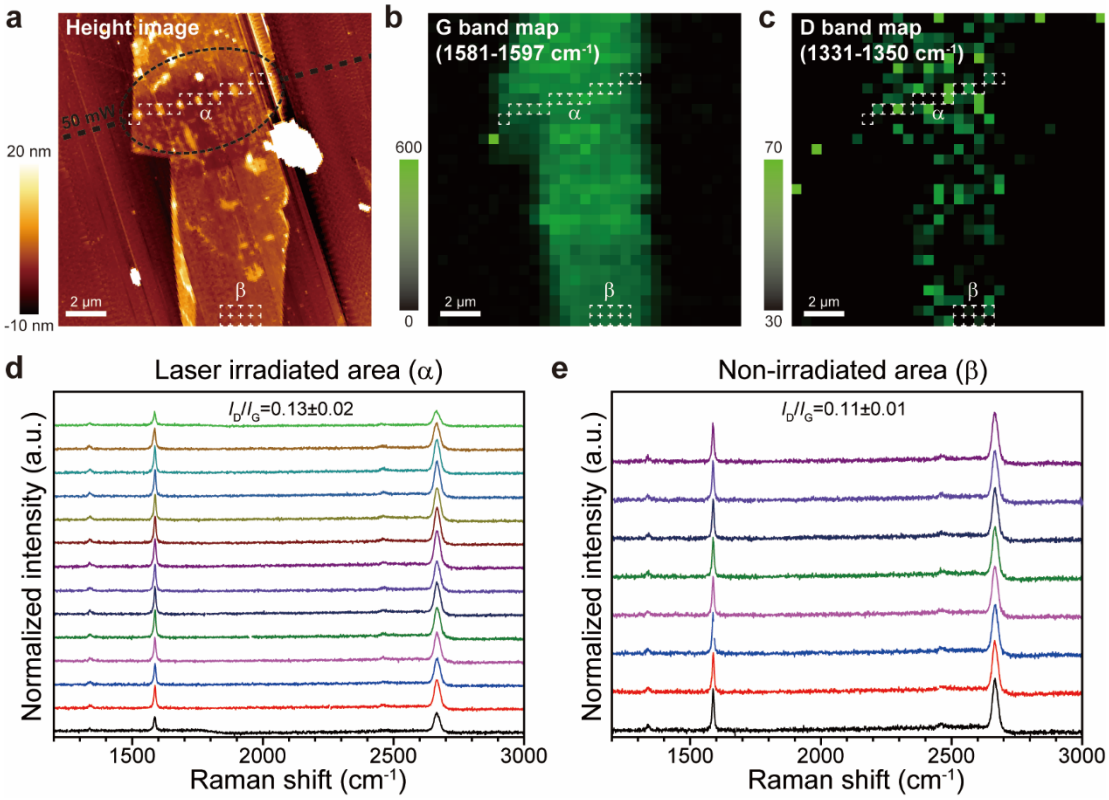

Figure S11. (a-e) Height profile comparison of graphene nanoballoons for laser irradiation (solid line), and four months after laser irradiation (dashed line).

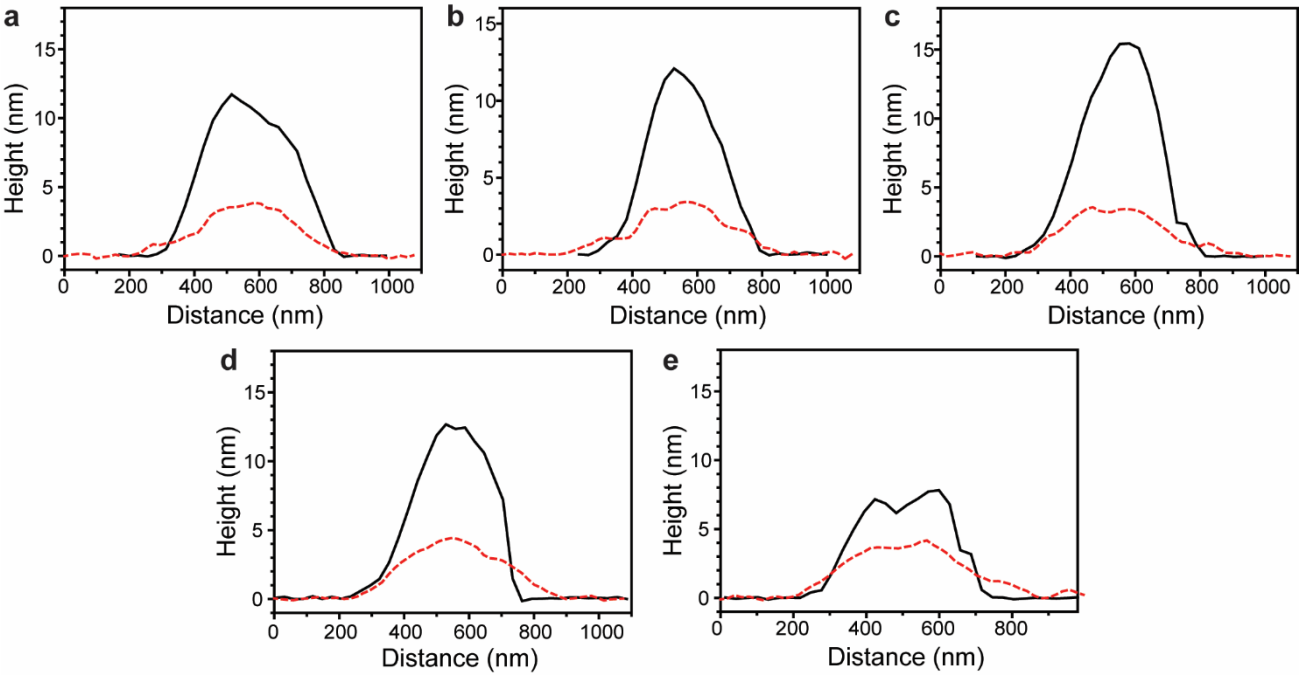

Figure S12. (a) Optical and (b) SEM images of graphene nanoballoons.

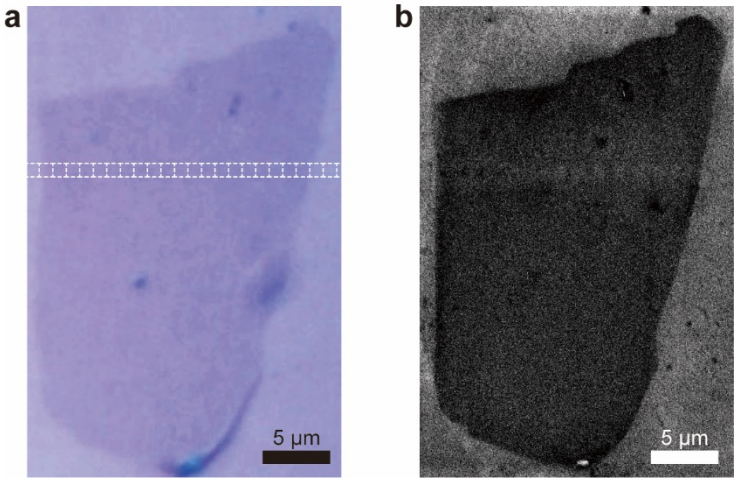

Table S1. Average ω_G and ω_{2D} with standard deviations according to t_{water}.

t_{water} [d]	ω_G		ω_{2D}	
	Average [cm^{-1}]	Standard deviation [cm^{-1}]	Average [cm^{-1}]	Standard deviation [cm^{-1}]
Annealed	1585.8	0.28	2681.1	0.38
2	1584.6	0.23	2679.5	0.28
4	1584.3	0.23	2679.0	0.35
7	1583.8	0.31	2678.1	0.40
24	1583.2	0.34	2676.0	0.50
42	1584.2	0.44	2678.3	0.52
75	1583.1	0.54	2675.7	1.03

Table S2. Physical parameters of nanoballoons and their exerted P and E.

Physical properties	Entry number					Average value
	1	2	3	4	5	
h (nm)	11.7	12.1	15.4	12.7	7.8	11.9
R (nm)	259	264	293	274	220	262
P (MPa)	0.3	0.32	0.43	0.31	0.18	0.31 ± 0.08
E (mJ/m^2)	1.42	1.50	2.6	1.55	0.55	1.52 ± 0.65

Cited references

[S1] W. Zhou, K. Yin, C. Wang, Y. Zhang, T. Xu, A. Borisevich*, et al.*, The observation of square ice in graphene questioned, Nature 528(7583) (2015) E1-E2.

[S2] K. Yue, W. Gao, R. Huang, K.M. Liechti, Analytical methods for the mechanics of graphene bubbles, J. Appl. Phys. 112(8) (2012) 083512.

[S3] H. Ghorbanfekr-Kalashami, K.S. Vasu, R.R. Nair, F.M. Peeters, M. Neek-Amal, Dependence of the shape of graphene nanobubbles on trapped substance, Nat. Commun. 8(1) (2017) 15844.

[S4] C. Lee, X. Wei, J.W. Kysar, J. Hone, Measurement of the elastic properties and intrinsic strength of monolayer graphene, Science 321(5887) (2008) 385-388.